Structural Studies of Metal Ions in Family II Pyrophosphatases: The Requirement for a Janus Ion[†,‡]

Igor P. Fabrichniy,[⊗,§] Lari Lehtiö,[⊗,#,§] Anu Salminen,[∥] Anton B. Zyryanov,[⊥] Alexander A. Baykov,[⊥] Reijo Lahti,[∥] and Adrian Goldman[*,⊗]

Program in Structural Biology and Biophysics, Institute of Biotechnology, University of Helsinki, P.O. Box 65, FIN-00014, Helsinki, Finland, National Graduate School in Informational and Structural Biology, Department of Biochemistry, University of Turku, FIN-20014 Turku, Finland, A. N. Belozersky Institute of Physico-Chemical Biology and School of Chemistry, Moscow State University, Moscow 119899, Russia

Received July 15, 2004; Revised Manuscript Received September 10, 2004

ABSTRACT: Family II inorganic pyrophosphatases (PPases) constitute a new evolutionary group of PPases, with a different fold and mechanism than the common family I enzyme; they are related to the "DHH" family of phosphoesterases. Biochemical studies have shown that Mn^{2+} and Co^{2+} preferentially activate family II PPases; Mg^{2+} partially activates; and Zn^{2+} can either activate or inhibit (Zyryanov et al., *Biochemistry*, *43*, 14395−14402, accompanying paper in this issue). The three solved family II PPase structures did not explain the differences between the PPase families nor the metal ion differences described above. We therefore solved three new family II PPase structures: *Bacillus subtilis* PPase (Bs-PPase) dimer core bound to Mn^{2+} at 1.3 Å resolution, and, at 2.05 Å resolution, metal-free Bs-PPase and *Streptococcus gordonii* (Sg-PPase) containing sulfate and Zn^{2+}. Comparison of the new and old structures of various family II PPases demonstrates why the family II enzyme prefers Mn^{2+} or Co^{2+}, as an activator rather than Mg^{2+}. Both M1 and M2 undergo significant changes upon substrate binding, changing from five-coordinate to octahedral geometry. Mn^{2+} and Co^{2+}, which readily adopt different coordination states and geometries, are thus favored. Combining our structures with biochemical data, we identified M2 as the high-affinity metal site. Zn^{2+} activates in the M1 site, where octahedral geometry is not essential for catalysis, but inhibits in the M2 site, because it is unable to assume octahedral geometry but remains trigonal bipyramidal. Finally, we propose that Lys205−Gln81−Gln80 form a hydrophilic channel to speed product release from the active site.

An essential enzyme in all living organisms is soluble inorganic pyrophosphatase (EC 3.6.1.1, PPase),[1] as it hydrolyzes PP_i to P_i (*1*). Surprisingly, there are two groups of PPases, family I and II, which are by both sequence (*2*, *3*) and structure (*4*, *5*) completely evolutionarily unrelated. Family I PPases are ubiquitous, occurring in all four kingdoms of life. The 57 nonredundant family II PPase sequences currently available in the GenBank are distributed in one unicellular eukaryote (*Giardia lamblia*), three archaeal, and 53 bacterial species. Family II PPases have been, in particular, found in 30 members of the eubacterial phylum Firmicutes such as *Bacillus subtilis* (Bs-PPase) and a variety of pathogens from *Clostridium*, *Staphylococcus*, and *Streptococcus* genera including *Streptococcus mutans*, which causes dental caries, *S. gordonii* (Sg-PPase), another oral bacterium, and *S. agalactiae* (*6*), which causes human neonatal pneumonia, sepsis, and meningitis. Furthermore, family II PPases are part of the "DHH" family of phosphoesterases originally identified by Aravind and Koonin (*7*), which includes *Drosophila melanogaster* Prune protein, *Saccharomyces cerevisiae* exopolyphosphatase, and *Escherichia coli* RecJ.

Despite the lack of sequence identity between family I and family II PPases, the structures of their active sites including the M^{2+}-water-M^{2+} activated nucleophile and the positions of P_i are very similar (*4*, *8*, *9*). The remarkable convergent evolution suggests that the chemical reaction mechanisms might also be similar. This is not, however, the case. Both family I and family II PPases catalyze the hydrolysis of $MgPP_i$, but the similarity ends there. The k_{cat} of family II PPases is ∼3000 s^{-1}; the k_{cat} for yeast PPase

[†] This work was supported by grants from the Academy of Finland (172168 and 178376 to A.G.; 201611 to R.L. and 1204363 to I.F.), by the Sigrid Juselius foundation, by the Russian Foundation for Basic Research (03−04−48798) and the Ministry of Industry, Science and Technologies of Russian Federation (1706−2003−4). L.L. is a member of the Informational and Structural Biology Graduate School.

[‡] Coordinates and structures factors have been deposited at the Protein Databank: 1WPM, 1WPN, and 1WPP.

* To whom correspondence should be addressed. AG (Institute of Biotechnology, Biocenter 3, Viikinkaari 1, P.O. Box 65, University of Helsinki, Helsinki FIN-00014, Finland. Phone: +358-(0)9-191 58923; fax: +358-(0)9-191 59940; e-mail: adrian.goldman@helsinki.fi.

[§] These two authors contributed equally to this work.

[⊗] University of Helsinki.

[#] National Graduate School in Informational and Structural Biology, University of Turku.

[∥] University of Turku.

[⊥] Moscow State University.

[1] Abbreviations: Bs-PPase, *Bacillus subtilis* inorganic pyrophosphatase; PPase, inorganic; pyrophosphatase; P_i, inorganic phosphate; PP_i, inorganic pyrophosphate; Sg-PPase, *Streptococcus gordonii* inorganic pyrophosphatase; Sm-PPase, *Streptococcus mutans* inorganic pyrophosphatase.

10.1021/bi0484973 CCC: $27.50 © 2004 American Chemical Society
Published on Web 10/23/2004

Table 1: Data Collection and Refinement Statistics

	Bs-PPase·Mn_2 core	Bs-PPase·S_i	Sg-PPase·$Zn_2(S_i)_2$
space group	$P2_1$	$P2_12_12_1$	$P2_12_12$
unit cell (Å,°)	48.1 × 61.0 × 74.1, $\beta = 100°$	59.7 × 117 × 145	96.1 × 149 × 43.7
wavelength (Å)	0.933	0.812	0.879
resolution (Å)[a]	20−1.3 (1.4−1.3)	30−2.05 (2.08−2.05)	20−2.05 (2.1−2.05)
no. of observations	486048	293841	179111
no. of unique reflections	195859	64380	74439
completeness (%)	96 (93,9)	98.8 (94.1)	97.8 (97.6)
R_{sym} (%)[b]	5.9 (41)	6.3 (40.8)	9.4 (35.6)
I/σ	18.4 (8.7)	28.7 (3.5)	8.4 (2.7)
resolution range (Å)	20−1.3	30−2.05	20−2.05
R-factor[c]	13.9	18.9	16.7
R_{free}[d]	16.6	24.8	21.6
test set (% of reflections)	5	5	5
no. of atoms	3593	5366	5338
average B values (Å^2)	15.9	34.4	22.6
rmsd from ideality:			
bond length (Å)	0.016	0.016	0.017
bond angle (°)	1.59	1.53	1.54
Ramachandran plot:			
favored (%)	91.2	90.9	89.8
allowed (%)	8.8	9.1	10.2

[a] Values in parentheses are for data in the highest-resolution shell. [b] $R_{sym} = \sum_i |I_i - \langle I \rangle| / \sum \langle I \rangle$, where I is an individual intensity measurement and $\langle I \rangle$ is the average intensity for this reflection with summation over all data. [c] R-factor $= \sum ||F_{obs}| - |F_{calc}|| / \sum |F_{obs}|$, where F_{obs} and F_{calc} are observed and calculated structure-factor amplitudes, respectively. [d] R_{free} is the R-factor based on a random 5% of the data withheld from refinement.

(Y-PPase), a family I enzyme, is 200 s^{-1} (*10*). Family I PPases bind and are activated by Mg^{2+} with micromolar affinity; family II PPases bind and are better-activated by Mn^{2+} with nanomolar affinity. However, the activity of family II PPase in the presence of Mg^{2+} is similar to that of family I PPase: Zyryanov (*11*) showed that Mg-activated Sg-PPase has the same k_{cat} as Mg-activated Y-PPase. The k_{cat} for Sg-PPase with Mn^{2+} is 15-fold higher because Mn^{2+} accelerates both PP_i hydrolysis and P_i release; furthermore, Sg-PPase binds neither PP_i nor P_i as tightly as Y-PPase. Other studies (*12*, *13*) have demonstrated that, consistent with structural results (*4*, *5*), Arg295 and Lys296 in family II PPase bind substrate.

The difference between family I and family II PPases may be in part due to the presence of His-ligands in the active site (*4*, *5*), which preferentially bind Mn^{2+} rather than Mg^{2+}, but other factors must also play a role. For instance, recent binding and mutagenesis studies (*10*) (Lahti, unpublished) indicate that only one of the two metal sites binds Mn^{2+} and Co^{2+} with nanomolar affinity. Furthermore, they show that Zn^{2+} binds with picomolar affinity, but activates the enzyme hardly at all (Zyryanov et al., accompanying paper in this issue). The domain closing that accompanies substrate binding and is presumably required for catalysis (*4*, *5*) (Fabrichniy, unpublished) may contribute to such effects.

To understand the basis of differential metal binding and catalysis, we have solved the structures of three family II PPases in different metalation states, which shed light on the complicated transition metal requirements for family II catalysis. We propose a structure-based explanation for why Zn^{2+} in lower affinity metal site (M1) activates the enzyme, but Zn^{2+} in the tight-binding site (M2) activates the enzyme hardly at all.

EXPERIMENTAL PROCEDURES

Protein Preparation and Crystallization. Bs- and Sg-PPases were expressed and purified as described previously (*10*). Protein concentrations were determined from UV absorbance on the basis of subunit molecular masses of 34.0 and 33.5 kDa and extinction coefficients $A_{280}^{1\%}$ of 2.64 and 3.43, calculated from the sequence of Bs- and Sg-PPase, respectively. The protein stock solutions, 35−40 mg/mL, contained 0.5 mM EGTA and 1 mM $MgCl_2$ in 150 mM Tris/HCl (pH 7.2) for Bs-PPase, or in 83 mM TES/K^+, 17 mM KCl (pH 7.2) for Sg-PPase.

To prepare Bs-PPase containing only Mn^{2+}, the protein stock was diluted 10-fold with 100 mM Tris/HCl buffer containing 2 mM EDTA and incubated for 4 h at +4 °C followed by two 30-fold dilution/reconcentration cycles on a Centricon YM-30 centrifugal filter device (Amicon), using 150 mM Tris/HCl buffer (pH 7.2) supplemented with 0.5 mM EGTA and 10 mM $MnCl_2$. To prepare Sg-PPase containing only Zn^{2+}, the protein stock was thrice diluted 10-fold and reconcentrated in 72 mM HEPES/K^+, 28 mM KCl buffer (pH 7.2). The solution was then made 100 μM in protein and 30 mM EDTA and incubated for 3 days at room temperature followed by six cycles of dilution/reconcentration in the same buffer (the first two cycles with 2 mM EDTA, the four last cycles with 10 μM EDTA). We then added 1.5 equivalents of $ZnCl_2$ to the resulting metal-free protein solution, followed by two dilution/reconcentration cycles in a buffer containing 20 μM $ZnCl_2$ and 10 μM EDTA. Before crystallization, the resulting Sg-PPase·Zn solution was incubated for 3 days with 10 mM $MgCl_2$ at +4° C.

Protein crystals were grown by sitting-drop vapor diffusion at + 4° C for Bs-PPase and at room temperature for Sg-PPase. Crystallization conditions were screened at 25−35 mg/mL protein concentration using standard screening methods (*14*, *15*). Large single rhombic crystals (1.0 × 0.8 × 0.5 mm) of intact Bs-PPase appeared within 3 days in a 3:2 mixture of protein stock:well solution (100 mM HEPES (pH 7.5), 2.3−2.5 M ammonium sulfate, 3−4% PEG 400) and diffracted to beyond 2.1 Å resolution (DESY, beamline X11) in space group $P2_12_12_1$ (Table 1). Another type of Bs-PPase crystal, clusters of needles (0.3 × 0.05 × 0.05 mm),

was obtained from protein stock stored at +4 °C for several months and mixed 1:1 with well solution containing 100 mM HEPES (pH 7.5), 2.4 M ammonium sulfate, and 3.3% PEG 400. The single crystals, when separated, diffracted to beyond 1.3 Å resolution (ESRF, beamline ID14−2) in space group $P2_1$, but contained only the N-terminal core due to proteolysis, and we refer to them below as "Bs-PPase core". Crystals of Sg-PPase·Zn (0.2 × 0.1 × 0.05 mm) diffracting to beyond 2.1 Å (DESY, beamline BW7a) in space group $P2_12_12$ were grown after nucleation by streak seeding of the preequilibrated crystallization drop containing a 1:1 mixture of protein stock with well solution (100 mM sodium citrate (pH 5.6), 1.8 M ammonium sulfate, 100 mM K/Na-tartrate) using a chinchilla hair. The seeds were taken from the large cluster of needles which grew during preliminary screening under similar conditions.

Data Collection and Processing. Crystals were briefly transferred to mother liquor supplemented with 18% glycerol and flash-frozen in a boil-off liquid nitrogen stream. Initial survey diffraction data were collected using Cu Kα radiation on an RU300 Rigaku rotating anode generator fitted with confocal mirrors and an Raxis IV+ image plate detector. Synchrotron data were collected on beamline X11 (intact Bs-PPase) or BW7a (Sg-PPase) at EMBL-Hamburg Outstation, Germany, or on ID14-EH2 (Bs-PPase core) at the ESRF, Grenoble, France. Data were processed with XDS (*16*) or the HKL package (*17*) (Table 1).

Structure Solution and Refinement. The structures were solved by molecular replacement using the Sg-PPase·Mn structure (PDB code 1K20; (*5*)) as a search model either with CNS (Sg-PPase·Zn, intact Bs-PPase) (*18*) or with MOLREP from the CCP4 Program Suite (Bs-PPase·Mn core) (*19*, *20*). We refined the structures with CNS (*18*) using the MLF target, and checked and rebuilt the models using O (*21*). Water molecules were built with ARP/wARP (*22*). The final refinement (Table 1) used Refmac (*23*) from the CCP4 Program Suite (*19*). Structures were overlaid using RgbSup (P. M. D. Fitzgerald, unpublished program) and displayed in O. The maps were calculated with CNS and the figures were generated using PyMOL (*24*).

Description of the C-Terminal Domain Movement. The motions of the C-terminal domain relative to the N-terminal domain may be roughly divided into two planar components, which we defined as "opening" and "twisting". To give a numerical measure of each motion, we introduce the corresponding angles: between Cα atoms of the residues (in Bs-PPase numbering) 211−188−13 for opening, and between residues 244−149−13 for twisting. The residues 211 and 244 belong to the most opened and twisted regions of the C-terminal domain, respectively, the residue 188 is a hinge, and the active site residues 13 and 149 are from the most structurally conserved region of the N-terminal domain assigning the movement plane.

Evaluation of the Metal Site Geometry. To evaluate the geometry for Mn^{2+} and Zn^{2+} bound to the four-, five-, or six-coordinated PPase metal-binding sites, we used the methodology described by Harding (*25*) dealing only with angular distortion. We measured the angles at the metal cation between all coordinating ligands and compared them with the ideal angles for square planar, trigonal bipyramidal, square pyramidal, and octahedral geometries as appropriate. In the square planar, trigonal bipyramidal, or octahedral geometries, the ideal angles are defined, but for square pyramidal geometry we calculated the ideal angles relevant for each case thus: first we determined the mean of the four angles between the axial and equatorial ligands (i.e., their ideal value) and then used it to calculate the ideal values for the remaining angles (*25*). The rmsd (root-mean-square deviation) between the ideal geometry angles and those observed in the structures gives a measure of the correspondence to the tested coordination type. To decide between possible coordination numbers, we used a cutoff distance of 2.45 Å for an Mn^{2+}−ligand bond and 2.35 Å for Zn^{2+}−ligand bond derived from the study of metal−O, N atoms interactions in "small-molecules" (*25*, *26*).

RESULTS

Fold of the Bs-PPase·Mn Core, Sg-PPase·Zn and the Bs-PPase Metal-Free Structures. All three structures are very similar to our and others' previously solved family II PPase structures (*4*, *5*). The protein chain of the monomer folds into two domains, a larger N-terminal domain connected by a six-residue linker to a smaller C-terminal domain. In the structure of Bs-PPase core the C-terminal domains are missing. As the structures are so similar, we use the *B. subtilis* PPase numbering in what follows.

In all three structures, two protein monomers per asymmetric unit form the physiological dimer. The interface between them comprises a five-stranded parallel β-sheet from the N-terminal domain of each monomer (*4*, *5*); the individual five-stranded sheets are mutually antiparallel. The N-terminal domains form a rigid core and, as in the other structures (*4*, *5*), the C-terminal domains adopt a variety of different conformations with respect to the N-terminal domain. For the Sg-PPase·Zn and the Bs-PPase structures, the N-terminal domains of both A and B monomers are identical (rmsd/Cα of 0.15 to 0.24 Å), so, unless otherwise noticed, we will only discuss the A monomers. The active site is located at the domain interface, and the motion of the C-terminal domain (see discussion) presumably reflects the possible complexes through which the enzyme passes during the catalytic cycle.

Metal Ion Ligands. In earlier structures of Sm- and Sg-PPase (*4*, *5*), the metalation state of the protein has been unclear; for instance, Sm-PPase, purified and crystallized from ammonium sulfate, is slightly yellow and contained a mixture of iron and Mn^{2+} in the active site, presumably due to contaminating iron in the ammonium sulfate. We therefore took extensive steps, based on solution studies (*11*), to prepare only the metal ion complex of interest. The procedure for incorporating Mn^{2+} (K_d = 0.5 nM) into Bs-PPase (see Experimental Procedures) was designed to ensure that all other metal ions were removed before addition of Mn^{2+}. In confirmation, an anomalous difference Fourier map calculated at 2.0 Å resolution showed two 16−17 σ peaks/monomer at the positions of the metal ions (Figure 1). The procedure for incorporation of Zn^{2+} at 1−2 mol/mol of protein was even more thorough, as we wished to correlate the structures with the changes in solution data that occur on Zn^{2+} substitution (Zyryanov et al., accompanying paper in this issue). The Zn^{2+} sites were visible at 10−11 σ in an anomalous difference Fourier map calculated at 2.1 Å resolution (data not shown).

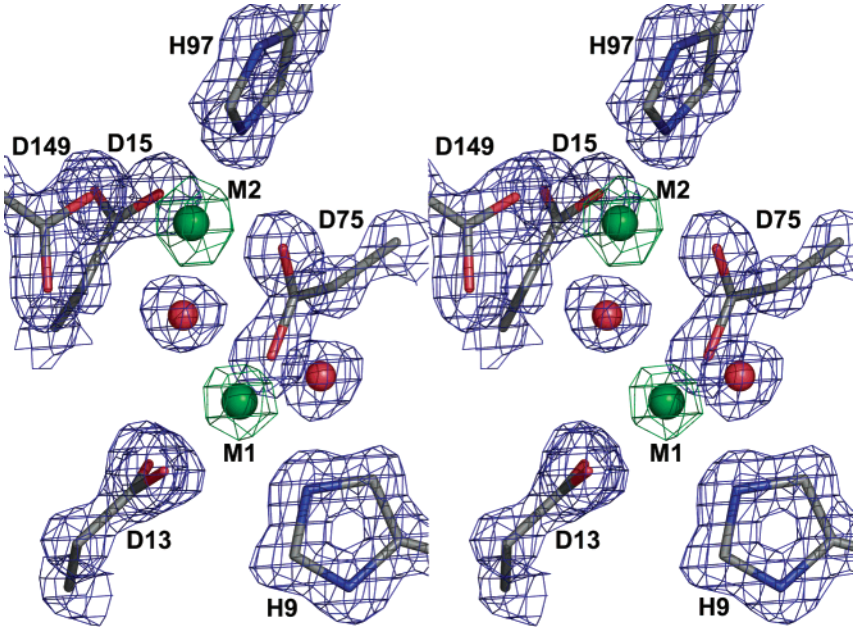

FIGURE 1: Mn^{2+} bound to the metal-binding sites in the active site of Bs-PPase·Mn_2 core. Stereoview of the refined sigmaA weighted $2F_o - F_c$ electron density composite omit map and anomalous difference Fourier map of the metal-binding sites of Bs-PPase core. The omit map is shown in gray contoured at 2σ and the anomalous map (10σ) is shown in green to highlight the large peaks associated with metals. The fit of the refined structure to the map is shown with atoms color coded by type: dark gray, carbon; blue, nitrogen; red, oxygen; and green, metal ions.

Table 2: Metal-Binding Geometries

			geometrical scores[c]				
enzyme	ligands[a]	assigned geometry[b]	sq. pl.	TBP	sq. pyr.	oct.	notes[d]
Bs core A	Mn1	TBP		7.9	12.2	(17.8)	D13 Oδ2 at 2.7 Å
	Mn2	TBP		8.0	12.8		
Bs core B	Mn1	TBP		8.4	11.6	(17.2)	D13 Oδ2 at 2.6 Å
	Mn2	TBP		8.2	12.4		
Sg A	Mn1	sq. pyr.		18.2	11.8	(21.1)	D13 Oδ1 at 2.5 Å
	Mn2	TBP/sq. pyr.		11.9	14.1		
Sg B	Mn1	sq. pyr.		25.4	22.8	(20.4)	H9 Nϵ2 2.6 Å
	Mn2	TBP/sq. pyr.		14.7	14.4		
Sg A	Zn1	sq. pl.	17.6			(18.7)	Wat at 2.6 Å; D13 Oδ2 at 2.5 Å
	Zn2	TBP		7.5	14.8		
Sg B	Zn1	sq. pl.	15.0			(16.8)	Wat at 2.6 Å; D13 Oδ2 at 2.5 Å
	Zn2	TBP		6.3	14.0		
Sm A	MnFe1 Sul1	sq. pyr.		12.5	8.6	(15.9)	D13 Oδ1 at 2.5 Å
	MnFe2 Sul1	oct				5.9	
Sm B	MnFe1 Sul1	distorted oct				18.6	Sul1 O1 at 2.4 Å
	MnFe2 Sul1	sq. pyr./oct		16.5	8.4	(10.3)	Sul1 O3 at 2.5 Å

[a] The numbers after the metals refer to site M1 and site M2. [b] Geometries: sq. pl. − square planar; TBP − trigonal bipyramid; sq. pyr. − square pyramid; oct. − octahedral. [c] Calculated as described in Experimental Procedures; values are shown for logical possible geometrical choices. [d] Ligand making long bond to the metal ion. The scores for the geometries including the long-bond ligand are given in parentheses.

The Bs-PPase·Mn Core Structure. The structure of the Bs-PPase·Mn core allows us to study the metal-binding sites with Mn^{2+}, the best enzyme activator, at 1.3 Å resolution (Figure 1), the highest so far for family II PPases. Studying Bs-PPase·Mn core is justified because its structure is very similar to intact protein, with an rmsd per Cα of 0.47 Å for the 187 N-terminal residues. The most flexible part of the N-terminal domain is a region preceding the hinge to the C-terminal domain (residues 150−188): it contains 50% of all residues with more than 0.3 Å deviation in their Cα positions. The other flexible regions are several short loops (not more than five residues), and none of them includes any active site residues participating in metal binding.

The metal sites are very similar to those in the Sg-PPase·Mn structure (*5*). M1 is bound by two water molecules, including the nucleophile Wat1, His9, the metal-ion bridge Asp75 and bidentately by Asp13 (Figures 1 and 2A). The Asp13 coordination is, however, not symmetric: the M1−Oδ2 distance is 2.66 Å (2.64 Å in monomer B), whereas the other distances are all 2.11−2.27 Å. The geometrical arrangement appears to be approximately trigonal bipyramidal (Table 2); the angles are 105−137° for equatorial ligands and 175° between the axial His9 and nucleophilic water molecule. Including Asp13 Oδ2, the coordination may be considered, as previously described (*5*), very distorted octahedral in monomer B (Figure 2A), but it appears to be square pyramidal in monomer A (Table 2).

The M2 site is even more clearly five-coordinate than the M1 site (Figure 2A). The M2 ligands are: the nucleophilic water Wat1, Asp15, Asp75, His97 and Asp149. The closest

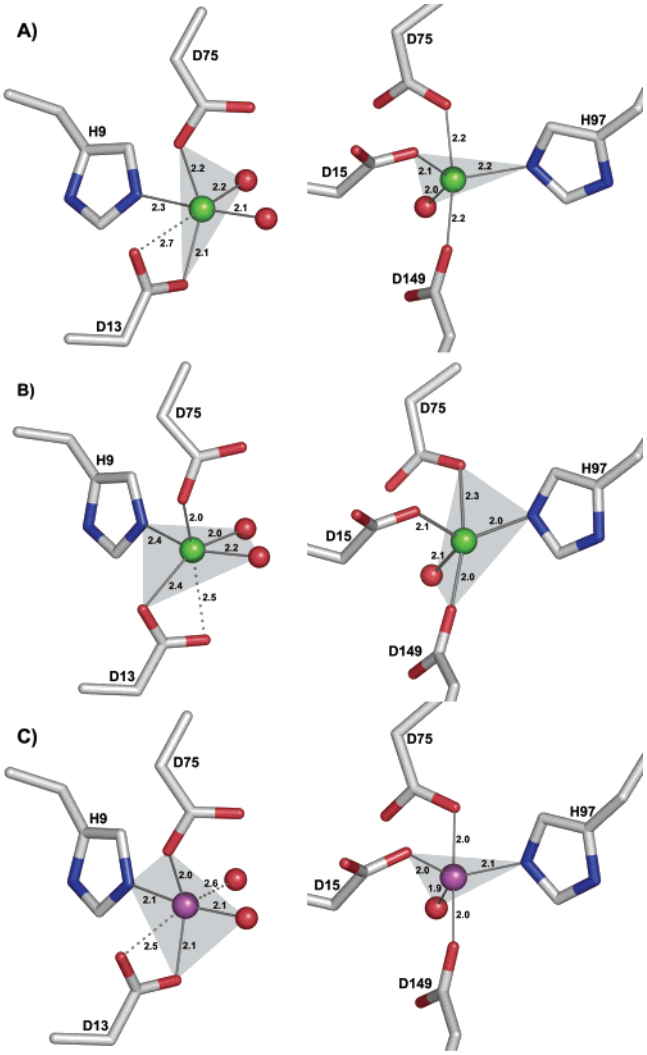

FIGURE 2: Different coordination geometry of the metal sites filled with Mn^{2+} and Zn^{2+}. Geometry of the metal-binding sites M1 (left column) and M2 (right column) observed in Bs-PPase·Mn_2 core (A), Sg-PPase·Mn_2S_i (B; *5*), and Sg-PPase·$Zn_2(S_i)_2$ (C) structures. Zn^{2+} is shown in magenta, Mn^{2+} is in green. The basal plane of the pyramidal geometry is shown in gray. The oxygen atoms of coordinating ligands are color coded red, the nitrogen atoms are color coded blue. Solid black lines illustrate short bonds to atoms in coordination positions and the corresponding bond lengths are indicated; dotted lines show additional possible coordination by atoms more than 2.5 Å from the metal ion.

plausible sixth ligand is Wat64, at 3.6 Å. The geometry of the M2 site has been described as square pyramidal for Sg-PPase·Mn (Figure 2) (*5*) but can equally as well be described as trigonal bipyramidal (Table 2; see below). Described that way, the three equatorial ligands are His97 Nϵ2, Wat1 and Asp15 Oδ2, with angles of 105−130° between the ligands. Interestingly, there is no sulfate bound to the metal sites, unlike in Sm-PPase (*4*), although the sulfate concentration in the crystallization solution was much higher.

The Sg-PPase·Zn Structure. The C-terminal domains in Sg-PPase·Zn have a different conformation compared to the previously solved Sg-PPase·Mn (*5*). In the A-monomer, the C-terminal domain is about 14° more opened from the N-domain than in Sg-PPase·Mn. This is similar to the open monomer (B) of Sm-PPase (*4*), but with the C-terminal domain about 0.5° more twisted, thus creating a wider channel to the active site (Figure 3A). The C-terminal domain in monomer B is a further 2.5° more open and 2° more twisted than in monomer A.

Each monomer contains two Zn^{2+} and three sulfate ions. One sulfate is bound at the solvent-exposed edge of each monomer close to the dimer interface and appears to be crystallographic. The active site contains two sulfates, one bound to the side chain of Arg295, and to the main-chain nitrogen 296 (Figure 3B). In the similar, but not identical, Sul2 site in Sm-PPase (*4*), additional bonds form; Arg295 makes a third bond with the sulfate through its main-chain nitrogen and Lys205 forms a bridge between sulfates Sul1 and Sul2. The second sulfate is bound to the side chains of Lys205, Gln81, and Gln80 in monomer A (Figure 3B), but only to Gln81 and Gln80 in monomer B. Lys205 and Gln81 are highly conserved (in 55/57 and 52/57 sequences, respectively) and Gln80 is partly conserved (21/57) among all known nonredundant family II PPase sequences. This Gln80−Gln81−Lys205 site, at the exit from the active site, has arisen because of the simultaneous opening and twisting of the C-terminal domain. Unlike in Sm-PPase, there is no sulfate bound at the Sul1 site to the metal ions. There are two Zn^{2+} bound to the active site of each monomer.

Zn^{2+} and Mn^{2+} (*5*) bind to Sg-PPase the same way, and similarly to how Mn^{2+} binds to the N-terminal core of Bs-PPase (see above). There are, however, important but subtle structural differences. Unlike Mn^{2+} in the M1 site in Sg-PPase (*5*) and in Bs-PPase core (above), Zn^{2+} in the M1 site appears to adopt a square planar geometry (Figure 2B). The two axial ligands (Wat90 and Asp13 Oδ2) are more than 2.5 Å from the Zn^{2+}, while the four planar ligands are 2.01−2.11 Å away. This is in agreement with its solution coordination preferences (*27*). M2, as in the Mn-containing structures (above; *5*), has only five ligands: Wat1, Asp15, Asp75, His97, and Asp149, but the geometry appears to be different (Figure 2C). Zn^{2+} in the M2 site appears to adopt trigonal bipyramidal coordination, while the Mn^{2+} geometry is somewhere between square pyramidal (*5*) and trigonal bipyramidal (above) (Figure 2A,B). We calculated the extent of distortion (*25*) of all the metal sites from perfect coordination geometries (Table 2). For Zn^{2+} in M2, the coordination is clearly trigonal bipyramidal; the rmsd is about 2-fold better than for square pyramidal (6.3−7.5 versus 14.0−14.8) (Table 2). The Mn^{2+} geometry in M2, on the other hand, conformed to neither ideal geometry (Table 2). The resting coordination state of Mn^{2+} in the M2 site is obviously significantly distorted from ideal.

We expect, however, that large coordination changes occur upon substrate/product binding. When the product analogue, sulfate, is bound to sites M1 and M2 (*4*), the five-coordinated geometry at M2 changes to octahedral (Figure 3C). This does not happen at M1, which remains square pyramidal with a long bond to Oδ1 of Asp13 (Table 2). The largest change is the position of the nucleophilic water molecule, which moves almost 1 Å perpendicular to the plane defined by M1, M2, and Cγ of Asp75 (Figure 3C). The motion is also directly away from the incoming sulfate group. As a result, the nucleophilic water becomes well-placed for catalytic attack. The Wat−P−O_{bridge} virtual angle becomes 170°.

The Bs-PPase Metal-Free Structure. We attribute the absence of Mg^{2+} to two factors: the high concentration of sulfate in the crystallization solution, and the moderate affinity (K_d = 88 μM) of the enzyme for Mg^{2+} (*10*). The

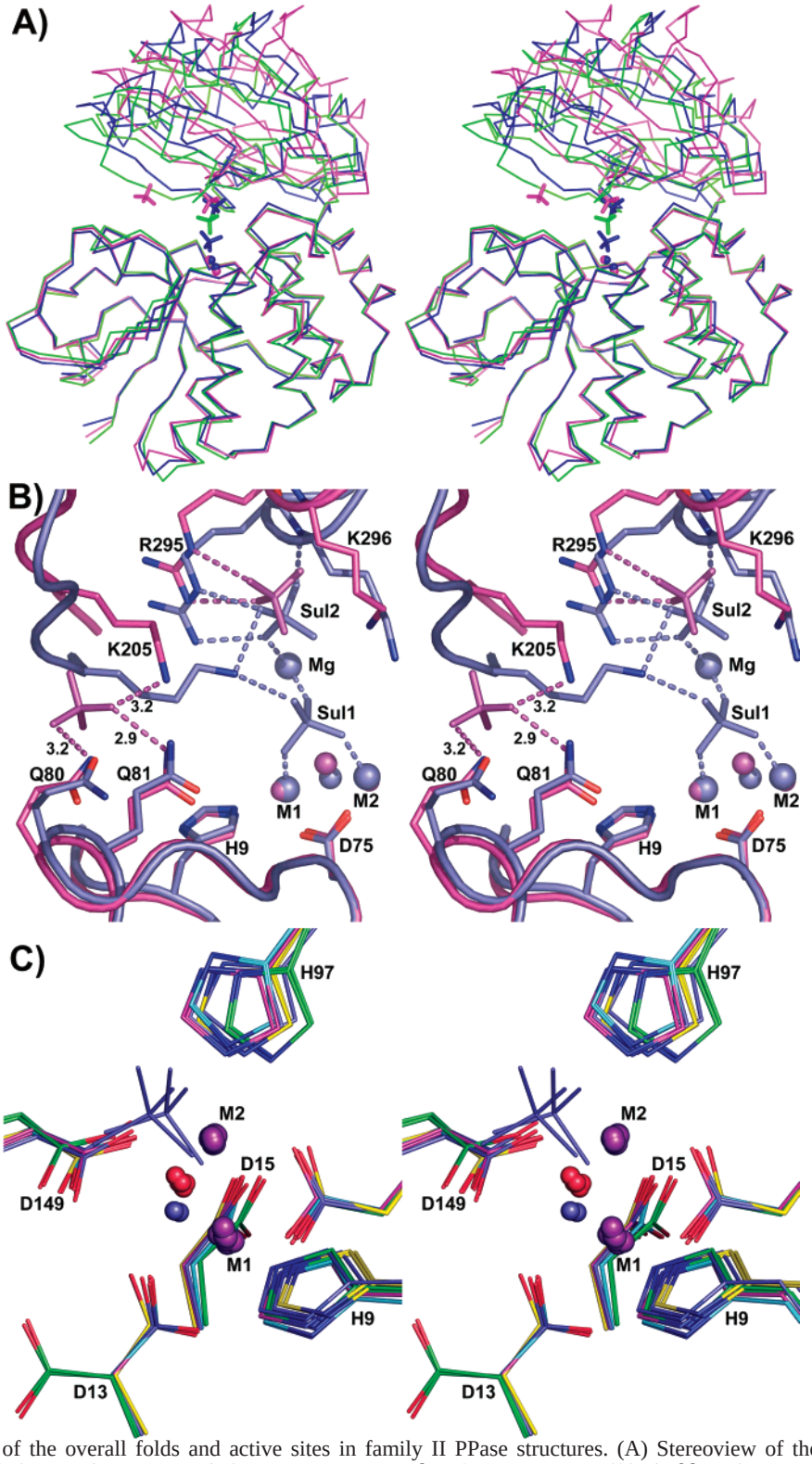

FIGURE 3: Comparison of the overall folds and active sites in family II PPase structures. (A) Stereoview of the Sg-PPase·$Zn_2(S_i)_2$ (in magenta) and Bs-PPase·S_i (in green) monomers A C_α-trace superimposed on Sm-PPase·$MnFe(S_i)_2$ (in blue, *4*) monomer A. Sulfate molecules are shown in sticks, metals in spheres and color coded for the respective structures. Structures are least-squares fitted by their N-terminal domains. The Sg-PPase·Mn_2S_i structure (not shown) folds similarly to Bs-PPase·S_i. (B) Stereoview of the superposition of the active sites of Sm-PPaseA·$MnFe(S_i)_2$ (blue) on Sg-PPaseA·$Zn_2(S_i)_2$ (magenta). The key active site residues Asp13 (Cα, Cβ, and Cγ), Asp15 (Cα) and Asp75 (Cα) were used. Sulfates are shown as sticks, metals as large spheres, and nucleophilic waters as smaller spheres color coded by structure. The Mg^{2+} ion in Sm-PPase, shown middle right, has no Sg-PPase counterpart. Residues specific to sulfate binding (see text) are labeled by amino acid code and sequence number; the respective bonds are shown in dashed lines with bond lengths. (C) Stereoview of the superposition of the metal-binding sites of both monomers of Sg-PPase·$Zn_2(S_i)_2$, Bs-PPase·Mn_2 core, Bs-PPase·S_i, Sm-PPase·$MnFe(S_i)_2$ and Sg-PPase·Mn_2S_i structures. The structures are least-squares fitted as in (B) excluding Cγ of Asp13 for fitting of Bs-PPase·S_i. Sg-PPase·Zn is in magenta, Bs-PPase·Mn_2 core in cyan, Bs-PPase·S_i in green, Sm-PPase in blue, and Sg-PPase·Mn_2 in yellow, and both monomers are identically colored. For Sm-PPase the sulfate in Sul1 site is shown in sticks, and the nucleophilic water as small spheres in blue. The nucleophilic water molecules in all other structures are small red spheres and the metal ions are larger violet spheres. The protein ligands of both metal sites are labeled by amino acid code and sequence number.

N-terminal domain is somewhat distorted in comparison with Sg-PPase, but the largest differences (2.5−3.5 Å) occur close to the two inserted residues in Sg-PPase (Ala30 and Gly69). The C-terminal domain is closed on the N-terminal domain as in Sg-PPase·Mn (*5*) and has a sulfate molecule bound to the Sul2 site, including side chains of Lys205 and Arg295, and to the main chain nitrogen of Lys296. The presence of a bond between the sulfate and Nϵ2 of His98 makes the sulfate binding identical to that observed in Sg-PPase·Mn (*5*).

The metal sites are, unsurprisingly, not perfectly preformed. The M1-binding side chain of Asp13 turns about 120 degrees away from its position in the metal-containing structures; two of the four protein ligands are thus lost and the binding site essentially ceases to exist. The changes in the M2 site are smaller, the biggest being that His97 moves about 1 Å toward the side chain of Asp75 and forms a tight (2.7 Å) hydrogen bond to it. This is clearly consistent with kinetic and equilibrium dialysis data showing that the two metal-binding sites have significantly different binding constants. Our structures thus suggest that M2 is the high-affinity metal-binding site, as it is the one with the smaller change upon metal binding. In the recently solved structure of metal-activated RecJ exonuclease (*28*), which also belongs to the DHH family of enzymes (*7*), the M2, not the M1, catalytic metal ion site is preserved. This also suggests that the M2 site is the high affinity one.

DISCUSSION

Substrate Binding and Product Release. Given the number of different family II PPase structures with sulfates in various positions (see above; *4*, *5*), what can be said about substrate binding and product release? As previously observed (*4*, *5*), the N-terminal domain contains the two activator metal sites, while the C-terminal domain binds directly to substrate. We start from the viewpoint that the closing of the C-terminal domain in different family II PPase structures presumably reflects enzyme−substrate/product complexes at different points along the catalytic pathway. The sulphate-containing structures clearly mimic product (P_i) release better than substrate (PP_i) binding.

The relevant structures to consider are Sm-PPaseA·MnFe(S_i)$_2$, Sm-PPaseB·MnFe(S_i)$_2$ (*4*), Sg-PPaseA·Zn$_2$(S_i)$_2$, Sg-PPaseB·Zn$_2$(S_i)$_2$, Bs-PPase·S_i (all this work) Sg-PPase·Mn_2S_i and Bs-PPase·Mn_2 (*5*), where PPaseA, PPaseB refer to A, B, monomers in a single structure when there is a difference, and the metalation and sulfation state of the active site is written out fully. First, all structures with a sulfate in the Sul2 site, Bs-PPase·S_i, Sg-PPase·Zn$_2$(S_i)$_2$, Sm-PPase·MnFe(S_i)$_2$, Sg-PPase·Mn_2S_i (Figure 3A) are at least partially closed; in other words, sulfate binding to the C-terminal domain is correlated with the closed conformation. Of the structures listed above, only Bs-PPase·Mn_2 (*5*) is fully open, and it does not contain sulfate. Conversely, our Bs-PPase·S_i structure is closed (Figure 3A), even though metals M1 and M2 are absent. The last step in product release, therefore (and presumably the first step in substrate binding), occurs at the Sul2 site, resulting in opening and closing of the C-terminal domain onto the bimetal site in the N-terminal domain. The absence of sulfate in the Bs-PPase·Mn_2 core structure even though the bimetal Sul1 site is fully formed also indicates that Sul1 is not the primary substrate-binding site. The structural data are thus in perfect agreement with the results of the oxygen exchange measurements (*11*) demonstrating that the first P_i released contains the incoming water.

As described before (*4*), the Sm-PPaseA·MnFe(S_i)$_2$ structure mimics the hydrolysis product complex, with both Sul1 and Sul2 bound. In the Sm-PPaseB·MnFe(S_i)$_2$, the Sul1 sulfate has already moved 0.5 Å away from the metals, and the C-terminal domain has opened by 8° and twisted by 13°. We propose that our Sg-PPase structures show the next two product release steps. In the Sg-PPaseA·Zn$_2$(S_i)$_2$ structure, the C-terminal domain has twisted a further 0.5°, and the most prominent change in the active site is the absence of a sulfate at Sul1. Instead, the exit channel, between the domains, contains a sulfate (Figure 3B). The highly conserved Lys205 (in 55/57 family II PPase sequences), rather than bridging sulfate molecules at Sul1 and Sul2, carries this sulfate (3.15−3.91 Å to three of the sulfate oxygens). The sulfate also forms the hydrogen bonds to Gln80 (conserved in 21/57 family II PPases, but highly conserved in Firmicutes, 21/23) and the highly conserved Gln81 (52/57). In Sg-PPaseB·Zn$_2$(S_i)$_2$, the sulfate does not interact with Lys205 (the shortest distance is 4.4 Å), but the interactions to Gln80 and Gln81 remain, as if the sulfate is leaving the active site. Sg-PPaseB·Zn$_2$(S_i)$_2$ is, consistent with this, a further 2.5° more open and 2° more twisted. Lys205−Gln81−Gln80 may thus provide the exit channel for the first product P_i to leave. Another consequence of Lys205 moving away from the active site is that the Sul2 binding site becomes weaker, as one of the ligands to the sulfate/phosphate at Sul2 is lost (Figure 3B). This may facilitate product release from the Sul2 site.

Gln80 and Gln81 may have, however, an alternative complementary role. In the closed conformation of the Bs-PPase·S_i structure, both Gln donate a hydrogen bond (2.7 and 3.1 Å, respectively) to the backbone carbonyl 206 O; similar interactions appear in the closed structure of Sg-PPase·Mn_2S_i (*5*) as well. They may thus be part of the mechanism for closing the active site and, more importantly, excluding water during catalysis (Fabrichniy, unpublished).

Metal Binding. Equilibrium dialysis, kinetic data, and mutagenesis show that Bs- and Sg-PPase bind the first Mn with 0.2−0.5 nM affinity, and the second much more weakly with millimolar affinity (*10*) (Lahti, unpublished). Comparison of the metal-free Bs-PPase·S_i structure with metal-containing structures, Sg-PPase·Mn_2S_i (*5*), core Bs-PPase·Mn_2, and Sg-PPase·Zn$_2$(S_i)$_2$, shows that the M2 site is preformed, but the M1 site is not (Figure 3C). The bidentate Asp13 M1 ligand is turned away, presumably significantly weakening the binding at site M1. Even when present, the Asp13 interaction is asymmetric: one bond, usually Asp13 Oδ2-M^{2+}, is always long (2.45−2.7 Å) in the Sg-PPase·Mn_2S_i, Sg-PPase·Zn$_2$(S_i)$_2$, and Bs-PPase·Mn_2 core structures. These are rather long Mn^{2+}/Zn^{2+} bonds to charged oxygen atoms (*26*), suggesting that the bond is weak. The coordinate geometry at M1 is unusual. In the Bs-PPase·Mn_2 core, it is trigonal bipyramidal; in Sg-PPase·Zn$_2$(S_i)$_2$, square planar and in Sg-PPase·Mn_2S_i, square pyramidal (Figure 2), although there are ligands at longer distances as well (Table 2). The M1 site apparently does not readily adopt ideal octahedral geometry, which may alter its metal ion affinity and have implications for catalysis (see below).

The biggest motion in the M2 site upon metal binding (comparing Bs-PPase·S_i with Bs-PPase·Mn_2 core) is a 1 Å motion of His97 away from Asp75 (Figure 3C). Other than that, the site changes little. However, the Mn^{2+} geometry at M2 is also not octahedral (Table 2), unlike in for example substrate-free Y-PPase·Mn_2 (*8*), muconate lactonizing enzyme (*29*) and arginase (*30*). The M2 site favors a very distorted square pyramidal or trigonal bipyramidal geometry except for nearly perfect trigonal bipyramidal Zn^{2+} in Sg-PPase·$Zn_2(S_i)_2$ (Table 2). This has implications for catalytic mechanism, substrate binding, and water activation.

Metal Ion Activation in Family II PPase: The Requirement for a Janus Ion. An unusual feature of family II PPases is their complex metal ion activation. Mn^{2+} is required as an activator (k_{cat} of 1700−3300 s^{-1}), and Mg^{2+} is not as effective (k_{cat} of 110−330 s^{-1}) whereas the K_m with Mg^{2+} is five times lower than with Mn^{2+} (10−30 μM versus 90−160 μM) (*10*). We earlier hypothesized that the preference for Mn^{2+} over Mg^{2+} in the active site was due to the presence of His ligands, Mn^{2+} being more permissive of histidine than Mg^{2+} (*4*). There appears to be a more subtle reason. In structures with sulfate or phosphate at Sul1 (*4*) (Fabrichniy, unpublished), the M2 coordination changes from five-coordinate square pyramidal (Mn^{2+}) or trigonal bipyramidal (Zn^{2+}) geometries to six-coordinate octahedral geometry (Mn^{2+} only). The situation is similar, although not as clear, at M1; in the absence of substrate, the geometry tends toward octahedral but with one or two very long (>2.45 Å) bonds. Activating metal ions, particularly at the tight-binding M2 site, should therefore be able to adopt five-coordinate geometries but prefer octahedral ones so as to drive the conformational change described above. Another consequence of the rearrangements upon sulfate binding is the displacement of the nucleophilic water molecule away from the bound sulfate, placing the nucleophile in a position more geometrically favorable for catalytic attack (Figure 3C). Presumably this shift of the nucleophilic water, which must be very tightly bound between the metals, is driven by the negatively charged oxygen atoms of the sulfate.

In addition, the ability of transition metal ions to return from six-coordinated, substrate-bound state, to the five-coordinated holo-enzyme state, should promote easier product release. In Sm-PPaseB·$MnFe(S_i)_2$, for instance, the metal geometry at M2 appears to be returning to square pyramidal (Table 2) as Sul1 leaves, consistent with our model. Finally, the model is in agreement with the rates of elementary catalytic steps (*11*) showing that Sg-PPase·Mn releases the first product 8−11-fold faster than Sg-PPase·Mg.

Zn^{2+} shows unique time-dependent activation followed by inhibition (Zyryanov et al., accompanying paper in this issue). Adding Zn^{2+} to metal-free PPase leads to a turnover rate of 10 s^{-1}, which is 200-fold less than adding Mn^{2+}. However, the addition of 1 equivalent of Zn^{2+} to PPase preincubated with 1 equivalent of Mg^{2+} (PPase·Mg) leads to a rapid increase in activity to the level of Mg-activated enzyme (200 s^{-1}), followed by a slow decrease to the Zn^{2+}-rate of 10 s^{-1}. This effect can be simply explained thus: the single Mg^{2+} in PPase·Mg binds to the high-affinity (K_d = 10−90 μM) (*10*) M2 site. Upon adding an equivalent of Zn^{2+}, the initial complex formed is PPase·$Mg^{site2}Zn^{site1}$. This is as active as PPase·Mg_2: the M2 metal ion is the activator, and its activity governs the activity of the enzyme. The binding constant of Zn^{2+} to the M2 site is 1.4 pM (Zyryanov et al., accompanying paper in this issue), so Zn^{2+} and Mg^{2+} change sites by mass action, generating PPase·$Zn^{site2}Mg^{site1}$. The activity of this species, now governed by Zn^{2+} as the M2 ion, is 10 s^{-1}. If, instead of Mg^{2+}, PPase is initially preincubated with Mn^{2+}, upon addition of Zn^{2+} the activity also increases but remains constant (Zyryanov et al., accompanying paper in this issue). Evidently Mn^{2+}, which binds to M2 10 000 times more tightly than Mg^{2+}, cannot be easily displaced by Zn^{2+}. Zn^{2+} activates, but only when bound to M1.

Why would Zn^{2+} at M2 prevent hydrolysis? Our current explanation is that it does not readily adopt the octahedral geometry required for catalysis. The preference of Zn^{2+} for four-coordinate (square planar) and five-coordinate (pyramidal) geometries is not problematic in M1, because none of the Mn^{2+} complexes (Figures 2 and 3C) are octahedral. However, M2 in the presence of sulfate/phosphate and Mn^{2+} or Mg^{2+} (Figure 3C) (*4*) (Fabrichniy, unpublished) is always octahedral. Conversely, the Sg-PPase·$Zn_2(S_i)_2$ M2 sites form perfect trigonal bipyramids (Table 2; Figure 2). The approach of PP_i to bind to M2 and form the sixth ligand would presumably be energetically unfavorable. Zn^{2+} should thus inhibit family II PPase chiefly by binding substrate more weakly, and this is experimentally borne out: there is a 5.5-fold increase in the Michaelis constant. The slightly decreased (1.7-fold) value of k_{cat} in the Zn-enzyme may be because Zn^{2+} at M1 and M2 do not favor the ∼1 Å shift in Wat1 to the correct position for nucleophilic attack upon substrate binding or does not effectively activate it (see above).

We now have a clearer model for why Mn^{2+} and Co^{2+} are preferred (*11*) in family II PPases over Mg^{2+} and Zn^{2+}. It is more than being able to accept His ligands. As important, if not more so, is flexible coordination geometry: the Janus-like ability to adopt five-coordinate pyramidal geometries in the native enzyme, but to convert easily to octahedral geometries upon substrate binding. Such changes may be important in product release and in other aspects of catalysis.

ACKNOWLEDGMENT

Beamtime was made available under the European Union Improving Human Potential Program (Access to Research Infrastructures), at EMBL/DESY Hamburg under contract No. HPRI-CT-1999-00017 and at the ESRF under contract No. HPRI-CT-1999-00022. We thank Drs. Andrea Schmidt and Elspeth Gordon for providing support at the EMBL/DESY and ESRF, respectively.

REFERENCES

1. Baykov, A. A., Cooperman, B. S., Goldman, A., and Lahti, R. (1999) in *Inorganic Polyphosphates* (Schröder, H. C., Ed.) pp 127−150, Springer-Verlag, Berlin.
2. Young, T. W., Kuhn, N. J., Wadeson, A., Ward, S., Burges, D., and Cooke, G. D. (1998) *Bacillus subtilis* ORF yybQ encodes a manganese-dependent inorganic pyrophosphatase with distinctive properties: the first of a new class of soluble pyrophosphatase?, *Microbiology 144*, 2563−2571.
3. Shintani, T., Uchiumi, T., Yonezawa, T., Salminen, A., Baykov, A. A., Lahti, R., and Hachimori, A. (1998) Cloning and expression of a unique inorganic pyrophosphatase from *Bacillus subtilis*: evidence for a new family of enzymes, *FEBS Lett. 439*, 263−266.
4. Merckel, M. C., Fabrichniy, I. P., Salminen, A., Kalkkinen, N., Baykov, A. A., Lahti, R., and Goldman, A. (2001) Crystal structure of *Streptococcus mutans* pyrophosphatase: a new fold for an old mechanism, *Structure 9*, 289−297.

5. Ahn, S., Milner, A. J., Futterer, K., Konopka, M., Ilias, M., Young, T. W., and White, S. A. (2001) The "open" and "closed" structures of the type-C inorganic pyrophosphatases from *Bacillus subtilis* and *Streptococcus gordonii*, *J. Mol. Biol. 313*, 797−811.
6. Rajagopal, L., Clancy, A., and Rubens, C. E. (2003) A Eukaryotic Type Serine/Threonine Kinase and Phosphatase in *Streptococcus agalactiae* Reversibly Phosphorylate an Inorganic Pyrophosphatase and Affect Growth, Cell Segregation, and Virulence, *J. Biol. Chem. 278*, 14429−14441.
7. Aravind, L., and Koonin, E. V. (1998) A novel family of predicted phosphoesterases includes *Drosophila* prune protein and bacterial RecJ exonuclease, *Trends Biochem. Sci. 23*, 17−19.
8. Heikinheimo, P., Lehtonen, J., Baykov, A. A., Lahti, R., Cooperman, B. S., and Goldman, A. (1996) The Structural Basis for Pyrophosphatase Catalysis, *Structure 4*, 1491−1508.
9. Heikinheimo, P., Tuominen, V., Ahonen, A.-K., Teplyakov, A., Cooperman, B. S., Baykov, A. A., Lahti, R., and Goldman, A. (2001) Towards a Quantum-mechanical description of Metal Assisted Phosphoryl Transfer in Pyrophosphatase, *Proc. Natl. Acad. Sci. U.S.A. 98*, 3121−3126.
10. Parfenyev, A. N., Salminen, A., Halonen, P., Hachimori, A., Baykov, A. A., and Lahti, R. (2001) Quaternary structure and metal ion requirement of family II pyrophosphatases from *Bacillus subtilis*, *Streptococcus gordonii*, and *Streptococcus mutans*, *J. Biol. Chem. 276*, 24511−24518.
11. Zyryanov, A. B., Vener, A. V., Salminen, A., Goldman, A., Lahti, R., and Baykov, A. A. (2004) Rates of Elementary Catalytic Steps for Different Metal Forms of the Family II Pyrophosphatase from *Streptococcus gordonii*, *Biochemistry 43*, 1065−1074.
12. Shizawa, N., Uchiumi, T., Taguchi, J., Kisseleva, N. A., Baykov, A. A., Lahti, R., and Hachimori, A. (2001) Directed mutagenesis studies of the C-terminal fingerprint region of *Bacillus subtilis* pyrophosphatase, *Eur. J. Biochem. 268*, 5771−5775.
13. Konopka, M. A., White, S. A., and Young, T. W. (2002) *Bacillus subtilis* inorganic pyrophosphatase: the C-terminal signature sequence is essential for enzyme activity and conformational integrity, *Biochem. Biophys. Res. Commun. 290*, 806−812.
14. Jancarik, J., and Kim, S.-H. (1991) Sparse matrix sampling: a screening method for crystallization of proteins, *J. Appl. Crystallogr. 24*, 409−411.
15. Cudney, B., Patel, S., Weisgraber, K., and Newhouse, Y. (1994) Screening and optimization strategies for macromolecular crystal growth, *Acta Crystallogr. D 50*, 414−423.
16. Kabsch, W. (1993) Automatic processing of rotation diffraction data from crystals of initially unknown symmetry and cell constants, *J. Appl. Crystallogr. 26*, 795−800.
17. Otwinowski, Z., and Minor, W. (1997) Processing of X-ray diffraction data in oscillation mode, *Methods Enzymol. 276*, 307−326.
18. Brunger, A. T., Adams, P. D., Clore, G. M., DeLano, W. L., Gros, P., Grosse-Kunstleve, R. W., Jiang, J. S., Kuszewski, J., Nilges, M., Pannu, N. S., Read, R. J., Rice, L. M., Simonson, T., and Warren, G. L. (1998) Crystallography & NMR system: A new software suite for macromolecular structure determination, *Acta Crystallogr. D 54*, 905−921.
19. CCP4. (1994) The CCP4 suite: Programs for protein crystallography, *Acta Crystallogr. D 50*, 760−763.
20. Vagin, A., and Teplyakov, A. (1997) MOLREP: an automated program for molecular replacement, *J. Appl. Crystallogr. 30*, 1022−1025.
21. Jones, T. A., Zou, J. Y., Cowan, S. W., and Kjeldgaard, M. (1991) Improved Methods for Building Protein Models in Electron Density Maps and the Location of Errors in these Models, *Acta Crystallogr. A 47*, 110−119.
22. Perrakis, A., Morris, R., and Lamzin, V. S. (1999) Automated protein model building combined with iterative structure refinement, *Nat. Struct. Biol. 6*, 458−463.
23. Murshudov, G. N., Vagin, A. A., and Dodson, E. J. (1997) Refinement of macromolecular structures by the maximum-likelihood method, *Acta Crystallogr. D 53*, 240−255.
24. DeLano, W. L. (2002) *The PyMOL Molecular Graphics System*, DeLano Scientific, San Carlos, CA.
25. Harding, M. M. (2000) The geometry of metal−ligand interactions relevant to proteins. II. Angles at the metal atom, additional weak metal-donor interactions, *Acta Crystallogr. D 56*, 857−867.
26. Harding, M. M. (1999) The geometry of metal−ligand interactions relevant to proteins, *Acta Crystallogr. D 55*, 1432−1443.
27. Harding, M. M. (2001) Geometry of metal−ligand interactions in proteins, *Acta Crystallogr. D 57*, 401−411.
28. Yamagata, A., Kakuta, Y., Masui, R., and Fukuyama, K. (2002) The crystal structure of exonuclease RecJ bound to Mn^{2+} ion suggests how its characteristic motifs are involved in exonuclease activity, *Proc. Natl. Acad. Sci. U.S.A. 99*, 5908−5912.
29. Helin, S., Kahn, P. C., Guha, B. L., Mallows, D. J., and Goldman, A. (1995) The Refined X-ray Structure of Muconate Lactonizing Enzyme from *Pseudomonas putida* prs2000 at 1.85 Å Resolution, *J. Mol. Biol. 254*, 918−941.
30. Kanyo, Z. F., Scolnick, L. R., Ash, D. E., and Christianson, D. W. (1996) Structure of a unique binuclear manganese cluster in arginase, *Nature 383*, 554−557.

BI0484973